JACS
JOURNAL OF THE AMERICAN CHEMICAL SOCIETY
Article
pubs.acs.org/JACS

Evaluation of Reoxidation Thresholds for γ-Al_2O_3-Supported Cobalt Catalysts under Fischer–Tropsch Synthesis Conditions

Nikolaos E. Tsakoumis,*[§] John C. Walmsley,[#,†] Magnus Rønning,[§] Wouter van Beek,[‡] Erling Rytter,[§] and Anders Holmen[§]

[§]Department of Chemical Engineering, Norwegian University of Science and Technology (NTNU), NO-7491 Trondheim, Norway
[#]Department of Physics, Norwegian University of Science and Technology (NTNU), NO-7491 Trondheim, Norway
[†]SINTEF Materials and Chemistry, NO-7465, Trondheim, Norway
[‡]Swiss-Norwegian Beamlines at ESRF, Grenoble F38043, France

Supporting Information

ABSTRACT: Size-dependent phenomena at the nanoscale influence many applications, notably in the science of heterogeneous catalysis. In cobalt-based Fischer–Tropsch synthesis (FTS), the size of Co nanoparticles (NPs) dictates to a high degree catalyst's performance in terms of activity, selectivity, and stability. Here, a highly dispersed Re/Co/γ-Al_2O_3 catalyst with high Co surface area per gram of catalyst was exposed to industrially relevant FTS conditions and monitored *in situ* by synchrotron X-ray radiation. X-ray absorption near-edge structure spectra were obtained on the cobalt K edge and Re L_3 edge of the working catalyst. The experimental results demonstrate development of tetrahedrally coordinated Co^{2+} forming at the expense of metallic $Co^{(0)}$. The structure of the oxide resembles $CoAl_2O_4$ and appears at the onset (first 5–10 h) of the reaction. Reoxidation of $Co^{(0)}$ is more pronounced close to the outlet of the reactor, where higher pH_2O is anticipated. The state of the Re promoter does not change during the FT process. We propose that reoxidation of small Co NPs is followed by spreading of Co oxide that leads to the formation of $Co_xAl_yO_z$ phases. Hence, in order to avoid an irreversible loss of the active phase during process start-up, catalyst design should be restricted to Co NPs larger than 5.3 nm.

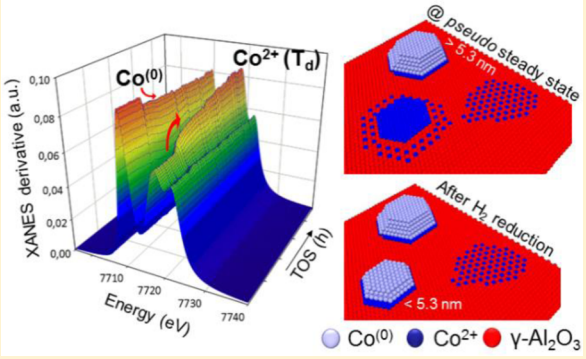

1. INTRODUCTION

Properties of nanoparticles (NPs) often exhibit strong size dependency at the nanoscale, and understanding such relations has a significant impact on heterogeneously catalyzed processes.[1] Rational design of heterogeneous catalysts based on a fundamental understanding of NP properties is necessary for improving the efficiency of chemical processes.[2] A prominent example of chemical process complexity that requires rational catalyst design for successful application is the Fischer–Tropsch synthesis (FTS). In FTS catalyzed by cobalt NPs, synthesis gas (a mixture of CO and H_2) is converted into high-quality hydrocarbons that can be further upgraded to ultraclean fuels and chemicals. In the recent years the process has attracted academic as well as industrial interest due to the alternative it offers for production of hydrocarbons from nonpetroleum feedstocks such as natural gas, coal, and biomass.[3,4]

Commonly, industrial Fischer–Tropsch (FT) catalysts consist of Co NPs dispersed on different refractory metal oxides, including TiO_2 and γ-Al_2O_3, doped with structural and reduction promoters.[5] High surface area supports like γ-Al_2O_3 are utilized for enhancing dispersion and maximizing available surface area of the active component. FTS has one of the most complicated chemical reaction environments, counting hundreds of products and intermediates deriving from surface oligomerization of CH_x building blocks, while high partial pressures of steam (pH_2O) are coproduced, rendering the reaction chemistry a challenging topic.

Structure sensitivity of the reaction limits the dispersion of the $Co^{(0)}$ active phase up to a threshold where activity (6 nm),[6−9] selectivity to higher hydrocarbons (8–9 nm),[10] and catalyst stability are not influenced.[11] In addition to the Co particle size sensitivity, the reaction is sensitive to the crystal structure of Co NPs[12,13] and the characteristics of the support.[14] Catalyst deactivation also appears more pronounced at high Co dispersions, while promoters may make a significant contribution to the observed deactivation rates.[15] Investigations of catalyst deactivation in such a complex and sensitive process have led to suggestions of different mechanisms,[11,16] the main ones being sintering, carbon formation, and reoxidation of Co. The latter has been a topic of scientific debate for the past 20 years.[15,17−20]

Received: November 17, 2016
Published: February 13, 2017

DOI: 10.1021/jacs.6b11872
J. Am. Chem. Soc. 2017, 139, 3706–3715

Former investigations on Co reoxidation have been conducted primarily by comparison of the state of activated against spent catalysts.[11] However, the added uncertainty of *ex situ* experimentation, together with air sensitivity of the activated material and the FT wax covering the spent catalyst, creates a demanding characterization challenge. Therefore, recent research has turned toward the equally challenging, but more reliable, *in situ* characterization at working conditions. The techniques that have been successfully applied for monitoring the state of Co *in situ* are X-ray absorption near-edge structure (XANES), X-ray powder diffraction (XRPD), magnetic methods, and Mössbauer spectroscopy.[21−24] Among them, XANES is the most sensitive to the oxidation state and co-ordination geometry of the absorbing atom, while it can give quantitative estimations of the involved phases.[25]

In the present study, a highly dispersed Re/Co/γ-Al_2O_3 catalyst with known particle size distribution (PSD) and an average Co NP size of 6.2 nm has been exposed to common benchmarking FTS conditions similar to those encountered inside an industrial reactor. Synchrotron-based X-ray radiation was utilized for *in situ* monitoring of the state of the active phase and promoter of the working catalyst, in order to shed light on phase transformations occurring during start-up and first day on stream.

2. EXPERIMENTAL AND ANALYTICAL PROTOCOLS

The γ-Al_2O_3-supported catalyst consists of 20 wt% Co and 0.5 wt% Re. It has been prepared by incipient wetness impregnation of a high surface area γ-Al_2O_3 (186 m^2/g, Puralox SCCa from Sasol GmbH) with a solution of cobalt nitrate and perrhenic acid in a mixture of H_2O and ethylene glycol added in a ratio of 0.9. After impregnation, the catalyst was dried (110 °C) for 3 h and calcined (300 °C) for 16 h. Sieved catalyst fractions of 53−90 μm were used for the experiment.

Transmission electron microscopy (TEM) measurements were performed with a JEOL 2100F instrument, operating at 200 kV accelerating voltage. The catalyst was reduced in a reactor cell at identical conditions to those applied in the *in situ* synchrotron experiment. The cell was purged with Ar, transferred and opened in a glovebox. Subsequently, the reduced catalyst was prepared by dispersion on a carbon-supported Cu mesh grid and then transferred to the TEM using a dedicated transfer holder. Particle size measurements were performed by direct measurements on the annular dark field STEM images using ImagJ. The longest radius of the NPs on a sample of 222 Co NPs was measured to derive the PSD. The contrast between NPs and support was variable, due to differences in thickness of the crushed fragments and overlap of projected images of neighboring particles. Care was taken to measure catalyst particles where it was judged that they could be observed individually with good atomic number contrast, bright relative to the support.

The *in situ* XANES experiment was performed at Station BM01B of the Swiss-Norwegian Beamlines (SNBL) located at the European Synchrotron Radiation Facility (ESRF) in Grenoble, France. X-ray absorption spectra were recorded at the Co K edge (E_0 = 7709 eV) and Re L_3 edge (E_0 = 10535 eV) by using a double-crystal Si (111) monochromator. Data collection was carried out in transmission mode. Gas-filled ion chamber detectors at ambient temperature and pressure were used for measuring the intensities of the incident (I_0) and transmitted (I_t) X-rays. The Co K edge E_0 is defined as 45% of the edge step, while the Re L_3 edge is defined as the maximum of the first derivative.

A quartz capillary-based *in situ* cell was used in a setup configuration similar to that described previously,[26,27] but modified to perform FTS at realistic conditions. A detailed description of the setup can be found elsewhere.[22,28] Initially, the calcined catalyst was diluted with one part of hexagonal boron nitride (h-BN) against three parts of catalyst and loaded into a quartz capillary (1 mm i.d.). High-temperature epoxy glue was used to seal the capillary and the metallic parts of the cell. Prior to the experiment, the system was flushed with pure H_2 at 25 °C. Reduction of the catalyst followed at 400 °C with H_2 flow of 2.5 mL/min at pressure slightly above atmospheric. The heating rate was set to 3 °C/min. The temperature was held at the set-point for 4 h before returning to 180 °C under the flow of He (5 mL/min). At 180 °C the system was pressurized to 18 bar using He diluted synthesis gas ($He:H_2:CO$ = 1.5:2.1:1). When the pressure was reached, the flow rates were adjusted to reaction levels ($He:H_2:CO$ = 0.5:2.1:1). The temperature was then increased at 1 °C/min to 220 °C. The catalyst was kept on stream at the chosen conditions for more than 24 h, after which the synthesis gas feed was replaced by He. The system was cooled down to room temperature and depressurized where post mortem profile analysis was performed.

The Athena software from the Ifeffit software package (Version 1.2.9)[29] was used for the X-ray absorption spectroscopy (XAS) data analysis. Data sets were processed as a unit with the same background correction and normalization parameters. A rhenium foil (thickness 0.0125 mm) and ReO_3 powder were used as references for the Re L_3 edge. Spectrum from a cobalt foil (hcp) was used as $Co^{(0)}$, and powder samples of pure Co_3O_4, CoO (rock-salt type), and $CoAl_2O_4$ were used as additional references. Co K edge XANES spectra were also simulated by the finite difference method and multiple scattering calculations. X-ray simulations were build using the finite difference method near-edge structure package FDMNES.[30] Identification and quantitative analysis of the Co phases has been done by a linear combination analysis (LCA) of first derivatives of normalized reference XANES spectra in the range −30 to +40 eV from the edge.

The commercially available Unscrambler X 10.2 software was used for the multivariate curve resolution-alternating least squares (MCR-ALS) data analysis. We have constrained the MCR analysis to non-negativity for normalized spectra and closure of concentration profiles. The number of pure components to be included in the MCR analysis was determined by principal component analysis (PCA) and examination of the signal-to-noise (S/N) and spectral structure of the components. A detailed description of application of MCR-ALS on full-range XAS can be found elsewhere.[31]

3. RESULTS

Freshly calcined catalyst consists of Co_3O_4 crystalline NPs, as detected by XRD (Figure 1), and Co K edge XANES (Figure S1). Co_3O_4 crystallites have an average size of 7 nm. The expected crystallite size of metallic Co NPs can be derived by taking into account shrinkage of the crystallites due to loss of oxygen from the lattice,[21] and it is estimated to be 5.6 nm. Lattice constants for cubic γ-Al_2O_3 and Co_3O_4 crystallites were

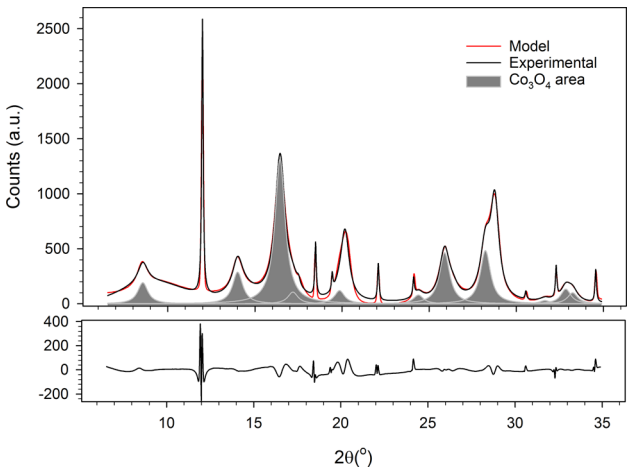

Figure 1. Full profile fit of the diffraction pattern obtained from the h-BN diluted Re/Co/γ-Al_2O_3 calcined catalyst (BM01A, ESRF λ = 0.6978 Å).

DOI: 10.1021/jacs.6b11872
J. Am. Chem. Soc. 2017, 139, 3706−3715

found to be 7.9474 and 8.0939 Å, respectively. Particularly for the γ-Al_2O_3 support, the unit cell appears significantly larger than that of the support before impregnation (7.9072 Å), suggesting that Co cation diffusion into the support is taking place during the calcination step.[32]

Co NP size analysis through H_2 chemisorption on the reduced catalyst gave an average size of 5.2 nm (11.9% Co dispersion and 16 m^2 $Co^{(0)}$/g). The product of catalyst reduction was quantitatively evaluated by XANES at the Co K edge. Spectra obtained from the reference compounds were combined linearly in all possible combinations and the best fit obtained is depicted in Figure 2a. The final degree of reduction

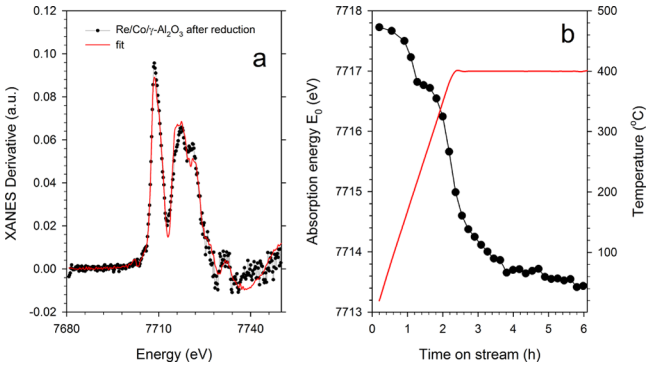

Figure 2. (a) LCA of the Co K edge XANES derivative spectra obtained at the end of reduction. (b) Shift in absorption edge $E_0(t)$ throughout reduction under pure H_2 (2.5 mL/min, 3 °C/min up to 400 °C and hold for 4 h).

of the catalyst is 91% (R-factor = 2.20 × 10^{-2}, χ^2 = 4.95 × 10^{-3}). During reduction the absorption edge (E_0) drifts toward lower values, meaning that the average oxidation state is moving toward zero. The shift is initiated at relatively low temperatures, near 160 °C, and extends for 4.4 eV. The low reduction initiation temperature implies that in the present NPs the reduction process are initiated earlier than for larger NPs for catalysts of similar composition,[22] in agreement with the TPR profiles of the two catalysts (Figure S1c). A similar observation was made for Co NPs with bimodal size distribution supported on carbon-based supports.[33]

In line with the known two-step reduction mechanism of Co_3O_4 that passes through CoO intermediate phase, two distinct regions, with different reduction rates, can be seen (Figure 2b). In the first region the rate evens out at 250 °C (Co_3O_4 to CoO) and triggered again at 315 °C until it levels out after 2 h at 400 °C (CoO to $Co^{(0)}$).

Comparison of rhenium L_3 edge spectra obtained at the start and at the end of the reduction shows that the Re promoter has been partially reduced under the applied conditions, Figure 3a. This is reflected in the decrease of "white line" intensity and simultaneous energy shift of approximately 3 eV that brings the E_0 edge position very close to that of the reference foil. Combination of the two aforementioned spectral characteristics suggests that, although Re is predominantly metallic, part of it still poses a cationic nature, probably due to interaction with the support as has been demonstrated for monometallic Re/γ-Al_2O_3 catalysts.[34] Since there is a linear relationship between the average formal oxidation state and the edge position,[35] an average oxidation state of +1.7 can be derived. This value is maintained during the FTS reaction at the steady state, Figure 3b.

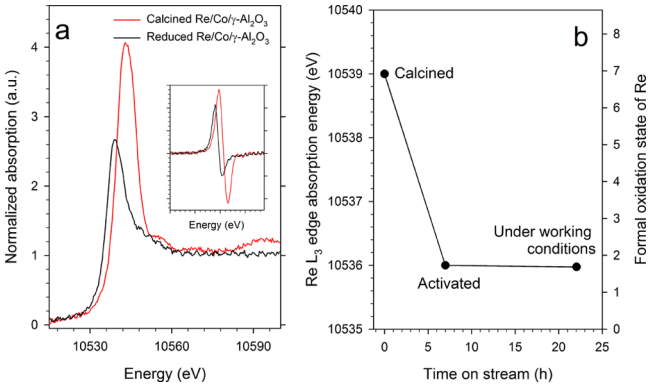

Figure 3. (a) Normalized XANES spectra at the Re L_3 edge and their first derivatives (inset). (b) Shift in absorption edge E_0 and average formal oxidation state of Re as evaluated from spectra obtained at different times on stream: before reduction (0 h, 25 °C), after reduction (7 h, 180 °C), and during FTS at pseudo steady state (22 h, 220 °C).

TEM analysis showed that Co NPs are finely distributed on the alumina support. The use of ethylene glycol during impregnation is known to allow a finer dispersion of Co on γ-Al_2O_3 inhibiting the formation of aggregates.[36] Such aggregates are absent in our standard TEM images; Figure 4a. Contrast consistent with a uniform distribution of Co

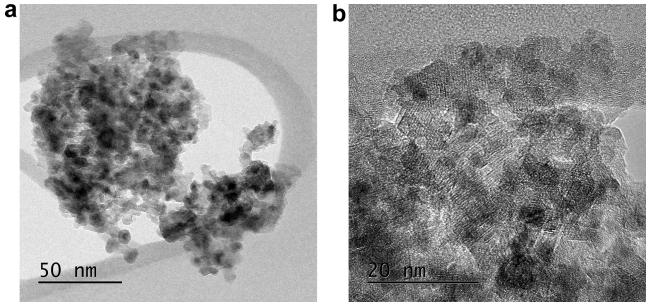

Figure 4. TEM image (a) and lattice resolution image (b) of the reduced catalyst after reduction at 400 °C for 4h (3 °C/min).

particles is seen. Furthermore, the lattice resolution images show no evidence of any common crystallographic orientation of Co NPs after reduction (Figure 4b), that is usually seen in aggregates of the Co_3O_4 phase in the calcined catalyst.[37] Figure 5 shows an example of the ADF-STEM images used for PSD measurements. The random distribution of the bright Co particles is evident in these images. The direct (number-weighted) PSD was converted to its volume-weighted equivalent (Figure 10S), since X-ray analysis gives a volume-weighted rather than a number-weighted or surface-weighted average.[38] Therefore, a volume-weighted distribution is expected to better correlate with the obtained average values from XANES spectra representing more precisely the sample. It should be mentioned here that atomically dispersed Co phases are not visible in such electron microscopy images and thus are not included in the obtained PSD.

The activated catalyst combines a high degree of reduction (91%) together with high dispersion of the active phase (11.9%) at high Co loadings (20 wt%), utilizing most of the catalytically active component.

Fischer–Tropsch Synthesis. After catalyst activation the system was cooled to 180 °C and pressurized. When the set-

DOI: 10.1021/jacs.6b11872
J. Am. Chem. Soc. 2017, 139, 3706–3715

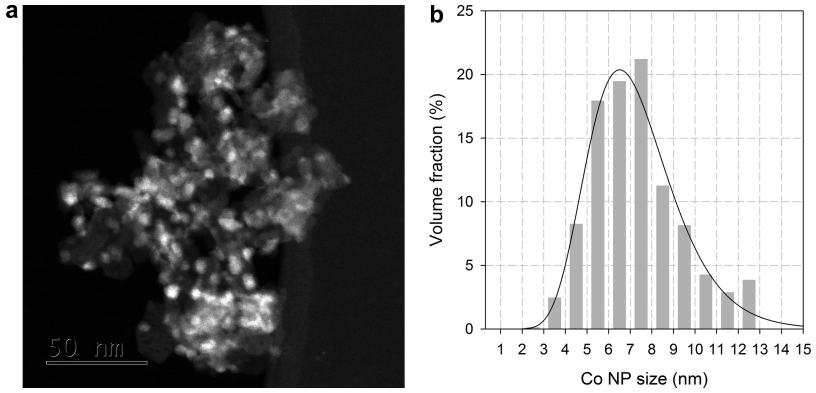

Figure 5. (a) Annular dark-field scanning transmission electron microscopy image (ADF-STEM) of the catalyst after reduction at 400 °C for 4 h (3 °C/min). (b) volume-weighted Co NP size distribution of the activated catalyst together with a log-normal fit on the data.

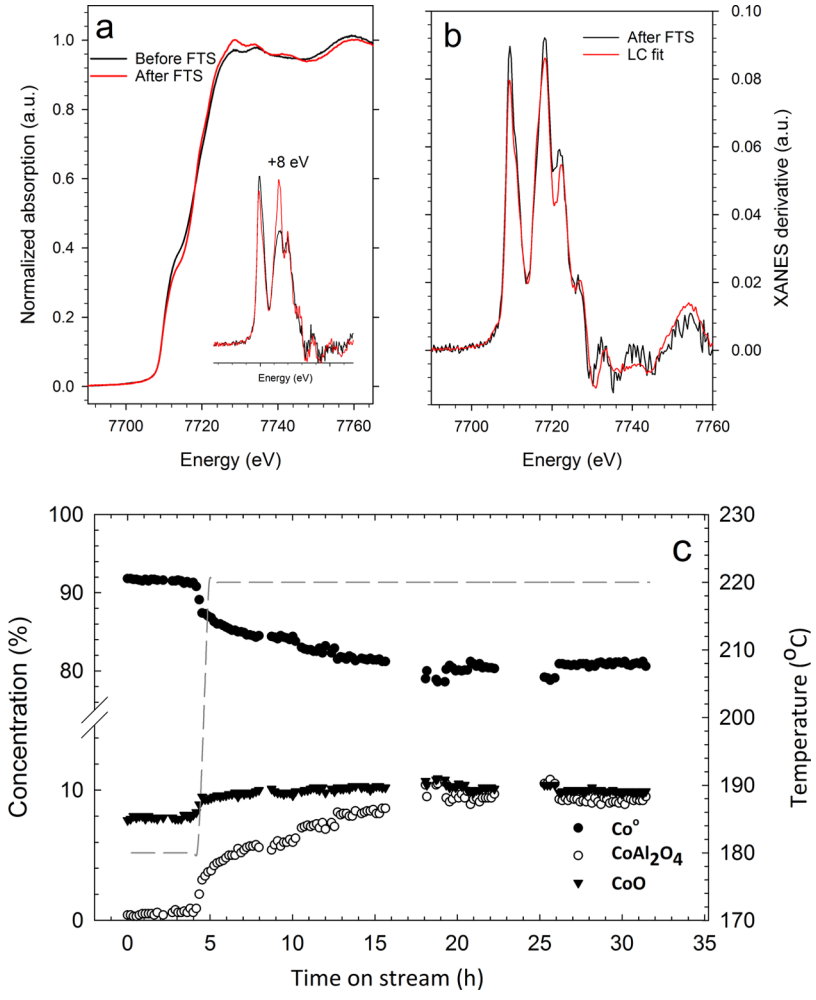

Figure 6. (a) Normalized XANES spectra and their corresponding first derivatives obtained before and after FTS. (b) First derivative spectrum after FTS and its fit by linear combination of the Co foil, CoO and $CoAl_2O_4$ bulk references. (c) LCA from the sequence of first derivatives of Co K edge XANES spectra obtained during reaction.

point pressure was reached, flows were adjusted and the temperature was increased at a rate of 1 °C/min to 220 °C. Subsequently FTS was performed for several hours. Estimation of the conversion level and the average reactor environment was done by comparison of the Re/Co/γ-Al_2O_3 catalyst with a reference catalytic material of the same composition that had been tested at identical conditions in lab-scale fixed bed reactor as well as in the *in situ* cell.[22] Despite their differences in dispersion (8.5% vs 11.9%), the two catalysts exhibit similar activity (r_{CO}= 0.53 mol CO/g*h) as demonstrated in fixed-bed reactor tests. Identical reaction conditions were chosen for the two catalytic materials and the results were extrapolated so as to estimate the conversion level (Figure S2). Consequently, CO conversion at the applied conditions inside the *in situ* cell is expected to reach 60−65% at pseudo steady state.

DOI: 10.1021/jacs.6b11872
J. Am. Chem. Soc. 2017, 139, 3706−3715

At the onset of FTS the reactor environment changes gradually. The initial dry conditions are followed by a significant shift in chemical potential with the formation of liquid products and high $pH_2O_{(g)}$. The prolonged induction period is possibly related to the implications that the change in chemical environment has on stabilization of the cobalt surface[39,40] and the gradual changes in diffusivity of products and reactants due to the formation of FT liquids.[41] Phase transformations and temperature stabilization issues may also interplay.[22,33]

Comparison of Co K edge XANES spectra obtained before the start and at the end of FT reaction shows significant changes; see Figure 6a. In the normalized XANES spectra, "white line" formation together with suppression of the shoulder in the rising edge are evident. In the corresponding derivatives, a noticeable increase in the feature +8 eV (7717 eV) above the edge is seen. The observation suggests reoxidation of cobalt into a phase rich in tetrahedrally coordinated (T_d) divalent cobalt (Co^{2+}).[42−44] Indeed, by observing the changes in absorption edge E_0 a drift toward higher energies is observed (Figure S3) supporting reoxidation of $Co^{(0)}$. The drift during the onset period is intense and levels off approximately after 5 h at the set-point temperature (220 °C). Evidently, reoxidation of Co NPs is taking place under the applied reaction conditions, but is limited only to the initial stages of the reaction.

Qualitative analysis by fitting and following representative features of the XANES derivatives for $Co^{(0)}$ (7709 eV), $CoAl_2O_4$ (7718 eV), and CoO (7722 eV) by Voigt functions shows significant changes of the derivative spectrum throughout FTS (Figure S3). The growth of both features at 7718 and 7722 eV with time is demonstrated, while the feature corresponding to $Co^{(0)}$ near the absorption energy (7709 eV) is decreasing. Results are in line with our previous observations[22] on a similar Co/Re/γ-Al_2O_3 catalyst with 10 nm average NP size, but much more pronounced, allowing a clear detection of the reoxidation phenomenon. All characteristic features of the XANES spectra i.e. E_0, white line and resonances; point toward reoxidation of $Co^{(0)}$.

Quantitative LCA utilizing Co K edge XANES spectra from bulk materials was used to reconstruct the derivative spectrum obtained after FTS (80% $Co^{(0)}$, 12% CoO and 8% $CoAl_2O_4$, R-factor = 1.67×10^{-2}, $\chi^2 = 3.00 \times 10^{-3}$), Figure 6b. Co foil, $CoAl_2O_4$, and CoO were chosen as representative standards as derived from PCA in combination with target transformation (Figure S6). In agreement with qualitative analysis, the output of the linear combination shows that 12% of $Co^{(0)}$ is consumed in favor of the formation of a Co^{2+} oxide. Consequently, the concentrations of $CoAl_2O_4$ and CoO increase during the FT process, with the first being the major developing phase (Figure 6c). LCA on the full data set describes the kinetics of the transformation, yet not all features of the derivative spectra could be reproduced during the fit. The difference between the formed compounds at the nanoscale against the bulk crystalline standards might explain the mismatch. Hence, a chemometric approach was applied in order to overcome this discrepancy.

MCR-ALS has been used traditionally to treat vibrational spectroscopy data[45,46] and only recently on XAS data.[31] The MCR-ALS chemometric analysis has been applied to the acquired data set combined with *ab initio* simulations of Co XANES spectra at K edge. Through MCR-ALS, fit statistics and analysis time are significantly improved since the full data matrix is analyzed as a unit, instead of analyzing single spectra. Thus, MCR is more suitable for large data sets providing faster output,[31] while the acquired components are allowed to relax within meaningful physicochemical constrains, such as non-negativity and closure (summation to 1 of the concentration profile), potentially supplying input on the mechanism and structure of the evolved phases. Both reference assisted (Figure S8) and blind source analysis were used (Figure S9).

Blind source analysis was applied to a matrix consisting of 163 spectra from pressurization, on-set and steady state FTS. The output of blind source analysis of the matrix is given in Figure 7. PCA analysis suggests that the data set can be decomposed into two main components. The contribution of a third component appears minor with increased noise levels (Figures S5 and S6). Comparison of the components with simulated and reference spectra shows strong similarities of the components with metallic Co and $CoAl_2O_4$. In particular, the first component shows spectral features similar to the ones found at $Co^{(0)}$ in a face-centered cubic (fcc) configuration (Figure 7c). It is well accepted, mainly from *in situ* XRD studies, that fcc-Co is the dominating crystal structure of Co NPs that have a size <20 nm and produced by H_2 reduction of Co_3O_4 NPs.[47] Contributions from other possibly existing phases like hcp-Co and rocksalt-CoO are probably part of the extracted component. For the second component, it becomes apparent that the formed phase clearly resembles in detail the $CoAl_2O_4$ structure; see Figure 7c. Both characteristic features of the T_d coordination, i.e. the pre-edge peak that corresponds to 1s → 3d transition, and electron resonances after ∼8−9 eV are found in the component, with especially the second to be more pronounced.[25]

An equally good fit is obtained when the components are compared with the metal−support mixed oxide phases ($Co_zAl_xO_y$) produced by the reduction of calcined γ-Al_2O_3 impregnated with low loadings of Co (3 wt%). Comparison with the simulated wurtzite-CoO that is composed solely from Co^{2+} (T_d), nor any other of the references (acquired or simulated), cannot describe the obtained component in such detail (Figure S7). Absorption edges of components 1 and 2 are located at 7710 and 7718 eV, respectively. Blind source analysis of the data set by the MCR-ALS provides a further proof of the formation of a $CoAl_2O_4$ like compound ($Co_xAl_yO_z$) during the initial stages of FTS as the final product of reoxidation. Observation of the extracted component concentrations shows clear loss of component 1 in favor of component 2. In accordance with the aforementioned LCA analysis, this result illustrates the transformation of a fraction of the activated catalyst, consisting of $Co^{(0)}$ and CoO phases into a final $Co_xAl_yO_z$ product. Contributions to the $Co_xAl_yO_z$ formation are from $Co^{(0)}$ that reoxidizes under FTS conditions and possibly from unreduced CoO reacting with the support as previously proposed.[48]

At the integral conditions applied (high conversions) the environment in a plug-flow reactor is position dependent (exhibits concentration gradient). As such, the outlet has higher $pH_2O_{(g)}$, and therefore it describes better the reaction environment inside widely applied slurry bubble column reactors (SBCR). An attempt was made to evaluate possible concentration gradients in the catalytic bed of the quartz capillary reactor. Thus, with the assistance of automated slits, the width of the X-ray beam was reduced to 1/3, and the different positions in the reactor were scanned (Figure 8). The first derivatives of the obtained Co K edge XANES spectra clearly demonstrate a more oxidized catalyst toward the outlet

DOI: 10.1021/jacs.6b11872
J. Am. Chem. Soc. 2017, 139, 3706−3715

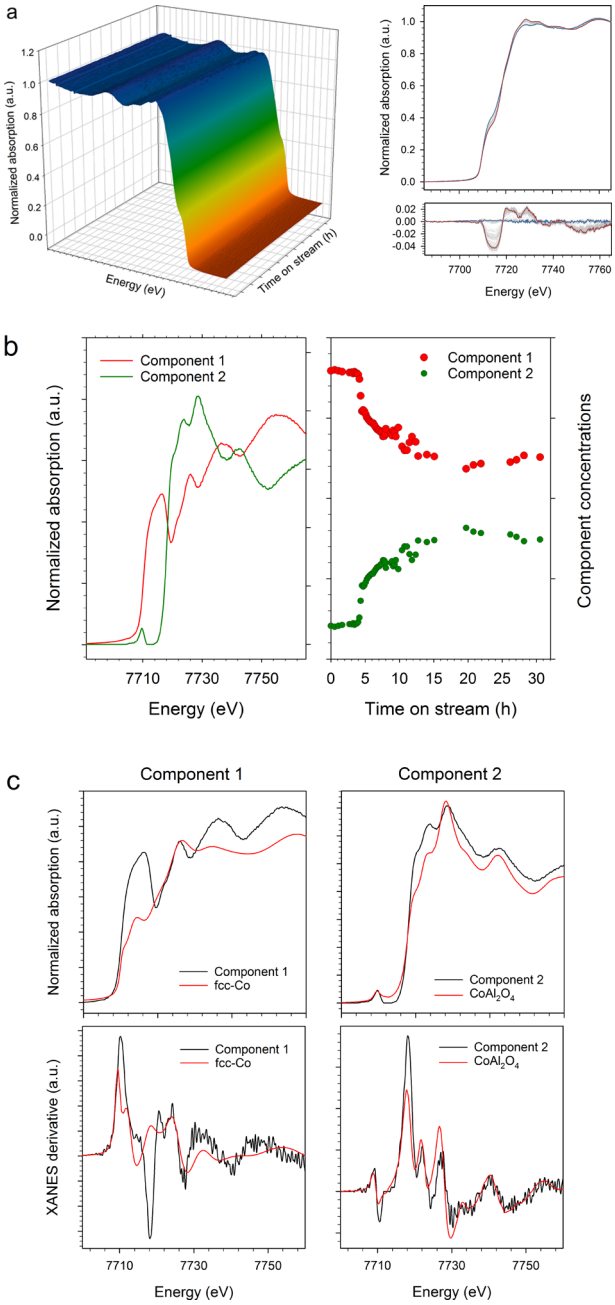

Figure 7. (a) 3D plot of normalized Co K edge XANES spectra obtained during reaction and normalized Co K edge XANES spectra obtained during reaction and their difference (ΔXANES). (b) MCR-ALS output with the corresponding extracted components of the blind source analysis and the dimensionless component concentrations. (c) Comparison of normalized and first derivatives of components 1 and 2 with simulated spectrum of fcc-Co, by the finite difference method, and powder $CoAl_2O_4$ reference, respectively.

of the catalyst bed. The feature at +8 eV after the edge is more pronounced while the feature at the edge position (7709 eV) is suppressed.

Similarly, normalized Co K edge XANES spectra show the "white line" formation. Our observation verifies a correlation of $pH_2O_{(g)}$ and formation of Co^{2+} compounds. Indeed, LCA shows that the degree of reduction after FTS is significantly lower at the reactor outlet (Figure 8b). In addition, by the spatially resolved analysis the existence and growth of a CoO intermediate phase is identified.

4. DISCUSSION

From Co K edge and Re L_3 edge XANES it is found that Co and Re species after activation resemble their corresponding zero-valent states. However, a small fraction of both elements preserves a positive charge, possibly due to strong interaction with the support. Furthermore, the current data set provides *in situ* evidence on the formation of Co^{2+} (T_d) at the initial stages of FTS performed at 220 °C, 18 bar and CO conversion in the order of 60%−65% (H_2:CO = 2.1). The transformation of $Co^{(0)}$ to Co^{2+} is clearly visualized in the onset of FTS (5−10 h) and levels off in the time scale where the system is expected to be in equilibrium (pseudo steady state). Since the reoxidation phenomenon is rapid and occurs only in the initial stages it is proposed that reoxidation should not be associated with catalyst deactivation.[11,49−54] Analogous observations were recently reported by X-ray absorption studies on *ex situ* obtained samples after catalyst activation and after the onset of FTS.[55] In addition, *in situ* magnetic measurements supported by *in situ* XRD during cofeeding of $H_2O_{(g)}$, simulating CO conversions of 77%, showed reoxidation of small Co NPs.[23] Similarly, the observed reoxidation was fast, lasting only a few hours. However, in both previous cases reoxidation led to the formation of cubic CoO. Here the reoxidation of the catalyst leads primarily to the creation of a phase similar to the $CoAl_2O_4$ compound comprised predominantly of Co^{2+} in tetrahedral coordination (T_d), as has been detected previously *ex situ* on Pt-promoted Co/γ-Al_2O_3 catalysts with similar extend of Co dispersion (11%).[56] A small part of the oxide in (O_h) Co^{2+} coordination, resembling cubic CoO, is also detected. The already existing CoO after reduction possibly participates in the observed formation of $Co_xAl_yO_z$.[48] The concentration of both oxides is higher toward the outlet of the reactor, evidencing the profound effect of pH_2O in this transformation. In accordance, Lögdberg et al. reported a rapid irreversible deactivation of small Co particles when high partial pressures of steam were externally introduced.[57]

Stabilization of the wurtzite-CoO phase, rich in Co^{2+} (T_d) at Co NPs < 4 nm under different environments has been reported recently by different research groups.[58−60] Authors argued the postulated Co-mixed compound formation during FTS to be related to wurtzite-CoO (Figure S7). In the current data set obtained under realistic FTS conditions neither the fit from LCA nor reference assisted MCR-ALS gave better results when the simulated XANES spectrum of wurtzite-CoO was used. Similarly, reoxidation during the induction period by C obtained from CO dissociation, that leads to Co_xC assemblies where C is covering step sites, cannot explain the extent of the present observations.[39] In addition, the XANES signal of the reoxidation product is far from known Co_xC structures (Figure S7).

Based on our observations a valid mechanistic scenario should fulfill two conditions. First is that the oxidation state is increasing from 0 to +2. Second, the final product of reoxidation is predominantly a $Co_xAl_yO_z$ structure. The magnitude of the observation suggests the existence of a mechanism that involves easy transfer of Co allowing the contact of cations with tetrahedral vacancies or other reactive sites in the surface of γ-Al_2O_3. Four different scenarios are discussed below.

DOI: 10.1021/jacs.6b11872
J. Am. Chem. Soc. 2017, 139, 3706−3715

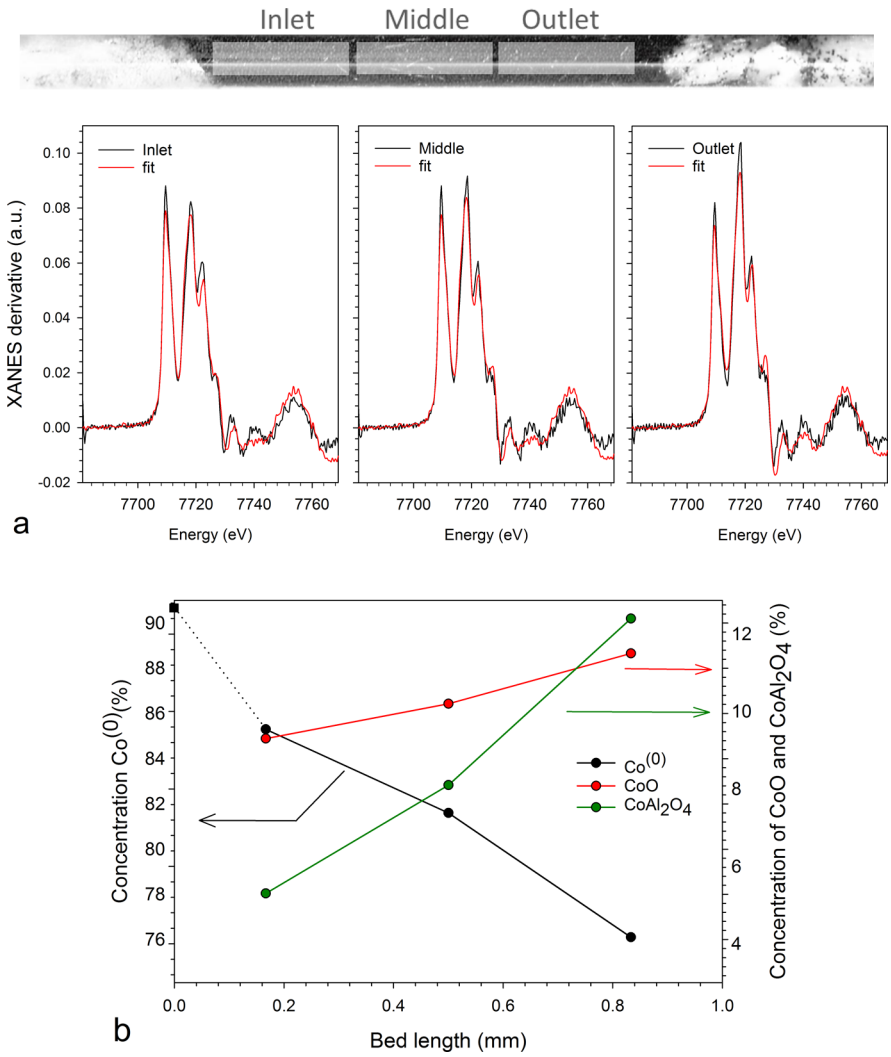

Figure 8. Post mortem profile analysis of the catalyst bed by Co-XANES at the K edge. (a) The obtained first derivatives together with the LCA fit of the inlet, middle, and outlet of the reactor are shown. (b) Quantitative results from the LCA.

(a) Static diffusion of Co atoms into the support through the interphase between support and NPs cannot alone describe the scale of the phenomenon. By assuming hemispherical Co NPs lying on the support the interfacial area between the NPs and the γ-Al_2O_3 can be calculated by dividing the Co surface area obtained by H_2 chemisorption (i.e., the area of the hemisphere $2\pi r^2$, where r is the radius) in half (since the base of the hemisphere has area equal to πr^2). Thus, only 6% of the Co atoms are at the interphase of NPs and γ-Al_2O_3. In addition, already during catalyst calcination and reduction[61] the loss of Co through diffusion into γ-Al_2O_3 is known to occur. Current Co K edge XANES data show that the DOR of the activated catalysts is 91%, while lattice constants obtained by XRD show that γ-Al_2O_3 in the calcined Re/Co/γ-Al_2O_3 catalyst has larger unit cell than of the material before the addition of Co. Both facts suggest that already in the activated catalyst there is a part of Co^{2+} that strongly interacts with the support, setting the path of static diffusion inadequate to explain the extent of reoxidation.

(b) Sole reoxidation of cobalt surface can be ruled out since a catalyst with 12% dispersion (meaning surface Co atoms) would be completely inactive at such severe reoxidation. This is not the case in the present catalyst, which exhibits similar activity to a catalyst with 8.5% dispersion. In addition, the final transformation of surface oxidized Co NPs into $CoAl_2O_4$ is difficult to visualize.

(c) Ostwald ripening was proposed to occur at the first 10 h of FTS[62] on planar Co/SiO_2 model catalysts under dry syngas conditions. The authors demonstrated that particles <5 nm decreased in size while the overall catalyst dispersion dropped. They suggested that Co forms sub-carbonyl monoatomic or small clusters that diffuse on the support and result in loss of total surface area. In such a scenario, especially for the initial reaction stage where pCO is at its maximum and temperature is comparably low to allow FT reaction ignition, sub-carbonyls could be favored. In addition, the highly defective surface of the γ-Al_2O_3 support would be partially dehydrated and therefore very reactive. Co atoms or clusters diffusing over the surface of the support might be captured by the support forming a Co oxide or being reoxidized by the conditions. This mechanism might contribute to the phenomenon, but profile analysis has shown that $p$$H_2O$ is more important than pCO, since

DOI: 10.1021/jacs.6b11872
J. Am. Chem. Soc. 2017, 139, 3706−3715

the $Co^{(0)}$ loss is higher toward the end of the reactor where pH_2O is maximized and pCO minimized accordingly.

(d) Finally, thermodynamic calculations have shown that bulk reoxidation of Co NPs can occur at FTS relevant pH_2O/pH_2 ratios for Co NPs less than 4.4 nm in diameter.[63] In the current case conditions during the observed reoxidation are milder (since steady state is not reached), yet dynamically capable of changing NPs energetics due to environmentally induced phenomena.[64,65]

In our view, the scenario of multilayer (bulk) reoxidation followed by Co oxide spreading on the γ-Al_2O_3 surface, allowing ultimately the reaction of Co^{2+} with the support, can explain the observations. Sub-carbonyl-assisted diffusion, merely during the initial stages of FTS, cannot be excluded and might have a contribution, while further ripening leads to particle growth.[66] Reaction-induced spreading is driven by the surface free energy difference of the NPs and support.[67−69] Spreading of CoO_x species over TiO_2 support in relation to FTS has been discussed previously.[58,70] In our case, the γ-Al_2O_3 support in its partially dehydroxylated state after reduction has indeed higher surface energy.[71] The production of $H_2O_{(g)}$ shifts the chemical potential inside the reactor and allows transformation of small metallic NPs to oxide forms.

Provided that the surface energy of the oxide NPs is lower than that of the support, Co NPs may spread on the surface of γ-Al_2O_3 and react, forming sub-monolayers of mixed metal−support compounds $Co_xAl_yO_z$ that resemble the $CoAl_2O_4$ structures (Figure 9). Metal−support interactions and strain are also known to affect the wetting/spreading properties.[67]

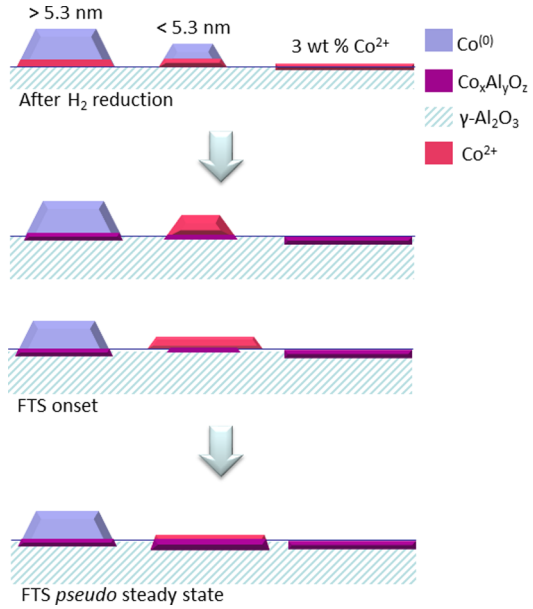

Figure 9. Illustration of the proposed reoxidation mechanism.

It is well accepted that γ-Al_2O_3 catalysts with low Co loadings (3%) lead to inactive materials.[72,73] Atomically dispersed Co shows epitaxial interactions with the support during aqueous impregnation that eventually leads to the formation of two-dimensional Co−Al oxide layered structures.[74,75] As already mentioned, highly dispersed Co-support phases are invisible by electron microscopic techniques meaning that they are not part of the Co PSD obtained by TEM. *In situ* X-ray diffraction has been used to probe them indirectly through the detection of their lattice expansion.[32,61] Here it is worth mentioning that an *in situ* XRD approach in the current case would give valuable input.

Based on the quantitative results that were obtained by the widely accepted LC fit, the establishment of a reoxidation threshold can be structured as follows. In our case, it can be assumed that from the 9% of cationic (+2) Co remaining in the reduced catalyst (from Co XANES) 6% is due to interfacial interaction of the Co NPs with the support (from H_2 chemisorption) and 3% of Co is existing in monolayer form and therefore is not included in the PSD (following refs 70−73), as described in the previous paragraph. Accordingly, our XRD patterns of the reduced catalyst support the absence of stand-alone CoO particles (Figure S1).

Therefore, it can be assumed that all the 91% metallic $Co^{(0)}$ is visible in TEM and by normalizing the continuous PSD to 91% the integrated area under the curve will correspond to the total number of TEM visible NPs. In our multilayer reoxidation scenario the 12% loss of $Co^{(0)}$ under benchmarking FTS conditions derived from the smallest $Co^{(0)}$ NPs with size less than 4.9 nm (bed average) and less than 5.3 nm in the extreme outlet conditions (Figure 10). As such, the threshold for

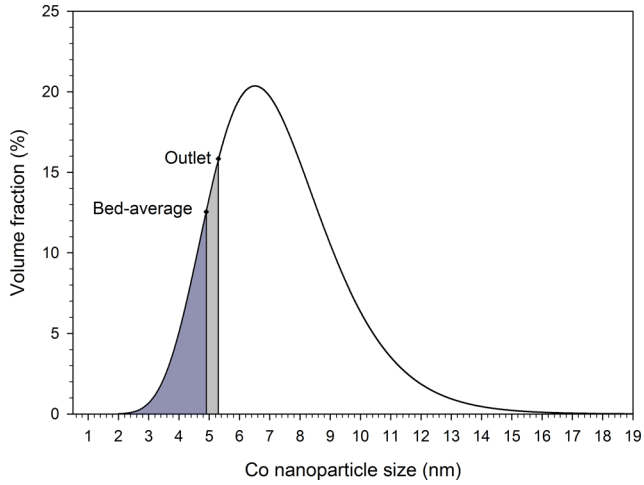

Figure 10. Reoxidation of Co NPs supported on γ-Al_2O_3 at the onset of FTS (220 °C, 18 bar, ~60% CO Conversion and H_2:CO = 2.1). Bed average reoxidation threshold for Co NPs 4.9 nm (blue area) and reoxidation threshold 5.3 nm for Co NPs at the outlet of the reactor (gray area).

optimized design avoiding reoxidation and Co-support compound formation $Co_xAl_yO_z$ can be set close to 5.3 nm with a sharp PSD above that limit. The threshold might be underestimated for slurry bubble column reactor applications that perform under higher pH_2O, since the reaction environment is dictated by outlet conditions due to significant back mixing.

5. CONCLUSIONS

We have provided experimental evidence on the reoxidation of Co NPs by applying *in situ* synchrotron X-rays on a Re/Co/γ-Al_2O_3 catalyst working at common FTS benchmarking conditions. Our data show that the highly dispersed Re-promoted metallic Co NPs supported on γ-Al_2O_3 partially reoxidizes to Co^{2+} principally in the initial stages of the FT

DOI: 10.1021/jacs.6b11872
J. Am. Chem. Soc. 2017, 139, 3706−3715

reaction. The formed Co^{2+} species adapt predominantly a $Co_xAl_yO_z$ structure, while rocksalt-CoO species are detected to a minor extent. A positive correlation between Co^{2+} formation and pH_2O was observed after analysis of the reactor profile. It also becomes apparent that the reactivity of the γ-Al_2O_3 support has a vital role in this phase transformation since the reoxidation product is not the CoO structure, but a compound very similar to $CoAl_2O_4$. At the pseudo-steady-state FTS conditions neither metallic Co nor Re species are altered.

Finally, we have demonstrated that *in situ* X-ray spectroscopy significantly benefit from chemometric analysis like the MCR-ALS protocol applied here. The powerful combination of quantitative information obtained from a single *in situ* experiment and the size distribution obtained by electron microscopy gives input to, and assists in, better catalyst design. In accordance, the minimum NP size for γ-Al_2O_3-supported Co-based FTS catalysts containing a promoter that provides a high degree of reduction has to be kept above 5.3 nm in order to avoid reoxidation.

■ ASSOCIATED CONTENT

Supporting Information

The Supporting Information is available free of charge on the ACS Publications website at DOI: 10.1021/jacs.6b11872.

Additional experimental procedures, results from computations, Figures S1−S10, and Tables S1−S3 (PDF)

■ AUTHOR INFORMATION

Corresponding Author

*tsakoumi@alumni.ntnu.no

ORCID

Nikolaos E. Tsakoumis: 0000-0002-3915-5937

Notes

The authors declare no competing financial interest.

■ ACKNOWLEDGMENTS

This publication forms a part of the *in*GAP (Innovative Natural Gas Processes and Products) Centre of Research-based Innovation, which receives financial support from the Norwegian Research Council under contract no. 174893. The SYNKNØYT programme by the Research Council of Norway is also acknowledged for support (grant no. 218406). The TEM work was carried out at the NORTEM Gemini Centre at NTNU and supported by the NORTEM project (grant no. 197405) within the INFRASTRUCTURE program of the Research Council of Norway. The personnel of the Swiss-Norwegian Beamlines, together with Dr. Alexey Voronov, are highly acknowledged for experimental assistance (experiment 01-01-868BM01B@SNBL).

■ REFERENCES

(1) Bell, A. T. *Science* **2003**, *299*, 1688.
(2) Arslan, I.; Walmsley, J. C.; Rytter, E.; Bergene, E.; Midgley, P. A. *J. Am. Chem. Soc.* **2008**, *130*, 5716.
(3) Fischer, F.; Tropsch, H. *Brennst.-Chem.* **1926**, *7*, 97.
(4) Khodakov, A. Y.; Chu, W.; Fongarland, P. *Chem. Rev.* **2007**, *107*, 1692.
(5) Rytter, E.; Ochoa-Fernández, E.; Fahmi, A. In *Catalytic Process Development for Renewable Materials*; Imhof, P., van der Waal, J. C., Eds.; Wiley-VCH Verlag GmbH & Co. KGaA: Weinheim, Germany, 2013.
(6) den Breejen, J. P.; Radstake, P. B.; Bezemer, G. L.; Bitter, J. H.; Frøseth, V.; Holmen, A.; de Jong, K. P. *J. Am. Chem. Soc.* **2009**, *131*, 7197.
(7) Barbier, A.; Tuel, A.; Arcon, I.; Kodre, A.; Martin, G. A. *J. Catal.* **2001**, *200*, 106.
(8) Bezemer, G. L.; Bitter, J. H.; Kuipers, H. P. C. E.; Oosterbeek, H.; Holewijn, J. E.; Xu, X.; Kapteijn, F.; van Dillen, A. J.; de Jong, K. P. *J. Am. Chem. Soc.* **2006**, *128*, 3956.
(9) Tuxen, A.; Carenco, S.; Chintapalli, M.; Chuang, C. H.; Escudero, C.; Pach, E.; Jiang, P.; Borondics, F.; Beberwyck, B.; Alivisatos, A. P.; Thornton, G.; Pong, W. F.; Guo, J.; Perez, R.; Besenbacher, F.; Salmeron, M. *J. Am. Chem. Soc.* **2013**, *135*, 2273.
(10) Rytter, E.; Tsakoumis, N. E.; Holmen, A. *Catal. Today* **2016**, *261*, 3.
(11) Tsakoumis, N. E.; Rønning, M.; Borg, Ø.; Rytter, E.; Holmen, A. *Catal. Today* **2010**, *154*, 162.
(12) Hofer, L. J. E.; Peebles, W. C. *J. Am. Chem. Soc.* **1947**, *69*, 2497.
(13) Liu, J.-X.; Su, H.-Y.; Sun, D.-P.; Zhang, B.-Y.; Li, W.-X. *J. Am. Chem. Soc.* **2013**, *135*, 16284.
(14) Borg, Ø.; Eri, S.; Blekkan, E. A.; Storsæter, S.; Wigum, H.; Rytter, E.; Holmen, A. *J. Catal.* **2007**, *248*, 89.
(15) Schanke, D.; Hilmen, A. M.; Bergene, E.; Kinnari, K.; Rytter, E.; et al. *Catal. Lett.* **1995**, *34*, 269.
(16) Saib, A. M.; Moodley, D. J.; Ciobîcă, I. M.; Hauman, M. M.; Sigwebela, B. H.; Weststrate, C. J.; Niemantsverdriet, J. W.; van de Loosdrecht, J. *Catal. Today* **2010**, *154*, 271.
(17) Hilmen, A. M.; Schanke, D.; Hanssen, K. K. F. F.; Holmen, A. *Appl. Catal., A* **1999**, *186*, 169.
(18) van de Loosdrecht, J.; Balzhinimaev, B.; Dalmon, J.-A.; Niemantsverdriet, J. W.; Tsybulya, S. V.; Saib, A. M.; Van Berge, P. J.; Visagie, J. L. *Catal. Today* **2007**, *123*, 293.
(19) Dalai, A. K.; Davis, B. H. *Appl. Catal., A* **2008**, *348*, 1.
(20) Saib, A. M.; Borgna, A.; van de Loosdrecht, J.; Van Berge, P. J.; Niemantsverdriet, J. W. *Appl. Catal., A* **2006**, *312*, 12.
(21) Rønning, M.; Tsakoumis, N. E.; Voronov, A.; Johnsen, R. E.; Norby, P.; van Beek, W.; Borg, Ø.; Rytter, E.; Holmen, A. *Catal. Today* **2010**, *155*, 289.
(22) Tsakoumis, N. E.; Voronov, A.; Rønning, M.; van Beek, W.; Borg, Ø.; Rytter, E.; Holmen, A. *J. Catal.* **2012**, *291*, 138.
(23) Fischer, N.; Clapham, B.; Feltes, T.; van Steen, E.; Claeys, M. C. M. *Angew. Chem., Int. Ed.* **2014**, *53* (5), 1342.
(24) Bezemer, G. L.; Remans, T. J.; Van Bavel, A. P.; Dugulan, A. I. *J. Am. Chem. Soc.* **2010**, *132*, 8540.
(25) Fernández-García, M. *Catal. Rev.: Sci. Eng.* **2002**, *44* (1), 59.
(26) Clausen, B. S.; Gråbæk, L.; Steffensen, G.; Hansen, P. L.; Topsøe, H. *Catal. Lett.* **1993**, *20*, 23.
(27) Couves, J. W.; Thomas, J. M.; Waller, D.; Jones, R. H.; Dent, A. J.; Derbyshire, G. E.; Greaves, G. N. *Nature* **1991**, *354*, 465.
(28) Urakawa, A.; Van Beek, W.; Monrabal-Capilla, M.; Galán-Mascarós, J. R.; Palin, L.; Milanesio, M. *J. Phys. Chem. C* **2011**, *115*, 1323.
(29) Ravel, B.; Newville, M. *J. Synchrotron Radiat.* **2005**, *12*, 537.
(30) Joly, Y. *Phys. Rev. B: Condens. Matter Mater. Phys.* **2001**, *63*, 125120.
(31) Voronov, A.; Urakawa, A.; van Beek, W.; Tsakoumis, N. E.; Emerich, H.; Rønning, M. *Anal. Chim. Acta* **2014**, *840*, 20.
(32) Arnoldy, P.; Moulijn, J. A. *J. Catal.* **1985**, *93*, 38.
(33) Tsakoumis, N. E.; Dehghan-Niri, R.; Johnsen, R. E.; Voronov, A.; van Beek, W.; Walmsley, J. C.; Borg, Ø.; Rytter, E.; Chen, D.; Rønning, M.; Holmen, A. *Catal. Today* **2013**, *205*, 86.
(34) Bare, S. R.; Kelly, S. D.; Vila, F. D.; Boldingh, E.; Karapetrova, E.; Kas, J.; Mickelson, G. E.; Modica, F. S.; Yang, N.; Rehr, J. J. *J. Phys. Chem. C* **2011**, *115*, 5740.
(35) Bare, S. R.; Ressler, T. Characterization of Catalysts in Reactive Atmospheres by X-ray Absorption Spectroscopy. *Advances in Catalysis*; Elsevier Inc.: Amsterdam, 2009; Vol. *52*, Chapter 6.
(36) Borg, Ø.; Dietzel, P. D. C.; Spjelkavik, A. I.; Tveten, E. Z.; Walmsley, J. C.; Diplas, S.; Eri, S.; Holmen, A.; Rytter, E. *J. Catal.* **2008**, *259*, 161.

DOI: 10.1021/jacs.6b11872
J. Am. Chem. Soc. 2017, 139, 3706−3715

(37) Borg, Ø.; Walmsley, J. C.; Dehghan, R.; Tanem, B. S.; Blekkan, E. A.; Eri, S.; Rytter, E.; Holmen, A. *Catal. Lett.* **2008**, *126*, 224.
(38) Beier, M. J.; Hansen, T. W.; Grunwaldt, J. D. *J. Catal.* **2009**, *266*, 320.
(39) Banerjee, A.; van Bavel, A. P.; Kuipers, H. P. C. E.; Saeys, M. *ACS Catal.* **2015**, *5*, 4756.
(40) Wilson, J. H.; de Groot, C. *J. Phys. Chem.* **1995**, *99* (20), 7860.
(41) Post, M. F. M.; Van't Hoog, A. C.; Minderhoud, J. K.; Sie, S. T. *AIChE J.* **1989**, *35*, 1107.
(42) Moen, A.; Nicholson, D. G.; Rønning, M.; Emerich, H. *J. Mater. Chem.* **1998**, *8*, 2533.
(43) Moen, A.; Nicholson, D. G.; Clausen, B. S.; Hansen, P. L.; Molenbroek, A.; Steffensen, G. *Chem. Mater.* **1997**, *9*, 1241.
(44) Bianconi, A.; Garcia, J.; Benfatto, M.; Marcelli, A.; Natoli, C. R.; Ruiz-Lopez, M. F. *Phys. Rev. B: Condens. Matter Mater. Phys.* **1991**, *43*, 6885.
(45) de Juan, A.; Tauler, R. *Crit. Rev. Anal. Chem.* **2006**, *36*, 163.
(46) Felten, J.; Hall, H.; Jaumot, J.; Tauler, R.; de Juan, A.; Gorzsás, A. *Nat. Protoc.* **2015**, *10*, 217.
(47) Kitakami, O.; Sato, H.; Shimada, Y.; Sato, F.; Tanaka, M. *Phys. Rev. B: Condens. Matter Mater. Phys.* **1997**, *56*, 13849.
(48) Moodley, D. J.; Saib, A. M.; Van De Loosdrecht, J.; Welker-Nieuwoudt, C. A.; Sigwebela, B. H.; Niemantsverdriet, J. W. *Catal. Today* **2011**, *171*, 192.
(49) Jacobs, G.; Patterson, P. M.; Zhang, Y.; Das, T. K.; Li, J.; Davis, B. H. *Appl. Catal., A* **2002**, *233*, 215.
(50) Jacobs, G.; Das, T. K.; Patterson, P. M.; Li, J.; Sanchez, L.; Davis, B. H. *Appl. Catal., A* **2003**, *247*, 335.
(51) Jacobs, G.; Das, T. K.; Li, J.; Luo, M.; Patterson, P. M.; Davis, B. H. *Stud. Surf. Sci. Catal.* **2007**, *163*, 217.
(52) Schanke, D.; Hilmen, A. M.; Bergene, E.; Kinnari, K.; Rytter, E.; Ådnanes, E.; Holmen, A. *Energy Fuels* **1996**, *10*, 867.
(53) Hilmen, A. M.; Schanke, D.; Hanssen, K.; Holmen, A. *Appl. Catal., A* **1999**, *186*, 169.
(54) Sirijaruphan, A.; Horváth, A.; Goodwin, J. G., Jr.; Oukaci, R. *Catal. Lett.* **2003**, *91*, 89.
(55) Jermwongratanachai, T.; Jacobs, G.; Shafer, W. D.; Ma, W.; Pendyala, V. R. R.; Davis, B. H.; Kitiyanan, B.; Khalid, S.; Cronauer, D. C.; Kropf, A. J.; Marshall, C. L. *Top. Catal.* **2014**, *57*, 479.
(56) Jacobs, G.; Das, T. K.; Patterson, P. M.; Li, J.; Sanchez, L.; Davis, B. H. *Appl. Catal., A* **2003**, *247*, 335.
(57) Lögdberg, S.; Boutonnet, M.; Walmsley, J. C.; Järås, S.; Holmen, A.; Blekkan, E. A. *Appl. Catal., A* **2011**, *393*, 109.
(58) Melaet, G.; Ralston, W. T.; Li, C.-S.; Alayoglu, S.; An, K.; Musselwhite, N.; Kalkan, B.; Somorjai, G. A. *J. Am. Chem. Soc.* **2014**, *136*, 2260.
(59) Zheng, F.; Alayoglu, S.; Guo, J.; Pushkarev, V. V.; Li, Y.; Glans, P.-A.; Chen, J.; Somorjai, G. A. *Nano Lett.* **2011**, *11*, 847.
(60) Papaefthimiou, V.; Dintzer, T.; Dupuis, V.; Tamion, A.; Tournus, F.; Hillion, A.; Teschner, D.; Hävecker, M.; Knop-Gericke, A.; Schlögl, R.; Zafeiratos, S. *ACS Nano* **2011**, *5*, 2182.
(61) Tsakoumis, N. E.; Johnsen, R. E.; van Beek, W.; Rønning, M.; Rytter, E.; Holmen, A. *Chem. Commun.* **2016**, *52*, 3239.
(62) Kistamurthy, D.; Saib, A. M.; Moodley, D. J.; Niemantsverdriet, J. W.; Weststrate, C. J. *J. Catal.* **2015**, *328*, 123.
(63) van Steen, E.; Claeys, M. C. M.; Dry, M. E.; van de Loosdrecht, J.; Viljoen, E. L.; Visagie, J. L. *J. Phys. Chem. B* **2005**, *109*, 3575.
(64) Hansen, P. L.; Wagner, J. B.; Helveg, S.; Rostrup-Nielsen, J. R.; Clausen, B. S.; Topsøe, H. *Science* **2002**, *295*, 2053.
(65) Zhang, H.; Gilbert, B.; Huang, F.; Banfield, J. F. *Nature* **2003**, *424*, 1025.
(66) Claeys, M. C. M.; Dry, M. E.; van Steen, E.; van Berge, P. J.; Booyens, S.; Crous, R.; van Helden, P.; Labuschagne, J.; Moodley, D. J.; Saib, A. M. *ACS Catal.* **2015**, *5*, 841.
(67) Knözinger, H.; Taglauer, E. *Handbook of Heterogeneous Catalysis*; Wiley-VCH Verlag GmbH & Co. KGaA: Weinheim, Germany, 2008.
(68) Wang, C.; Cai, Y.; Wachs, I. E. *Langmuir* **1999**, *15*, 1223.
(69) Kliewer, C. E.; Kiss, G.; Demartin, G. J. *Microsc. Microanal.* **2006**, *12* (2), 135.
(70) Cats, K. H.; Andrews, J. C.; Stéphan, O.; March, K.; Karunakaran, C.; Meirer, F.; de Groot, F. M. F.; Weckhuysen, B. M. *Catal. Sci. Technol.* **2016**, *6*, 4438.
(71) Navrotsky, A.; Ma, C.; Lilova, K.; Birkner, N. *Science* **2010**, *330*, 199.
(72) Lee, W. H.; Bartholomew, C. H. *J. Catal.* **1989**, *120*, 256.
(73) Jacobs, G.; Ma, W.; Davis, B. H. *Catalysts* **2014**, *4*, 49.
(74) Larmier, K.; Chizallet, C.; Raybaud, P. *Angew. Chem., Int. Ed.* **2015**, *54*, 6824.
(75) Wivel, C.; Clausen, B. S.; Candia, R.; Morup, S.; Topsøe, H. *J. Catal.* **1984**, *87*, 497.

DOI: 10.1021/jacs.6b11872
J. Am. Chem. Soc. 2017, 139, 3706−3715